What is the skill of ocean tracers in reducing uncertainties about ocean diapycnal mixing and projections of the Atlantic Meridional Overturning Circulation?

[1]

Marlos Goes* (1), Nathan M. Urban (1), Roman Tonkonojenkov (1),

Murali Haran (2), Andreas Schmittner (4), and Klaus Keller (1,3)

(1) Department of Geosciences, The Pennsylvania State University, University Park, U.S.A.

(2) Department of Statistics, The Pennsylvania State University, University Park, U.S.A.

(3) Earth and Environmental Systems Institute, The Pennsylvania State University,

University Park, U.S.A.

(4) College of Oceanic and Atmospheric Sciences, Oregon State University, Corvallis, U.S.A.

* Corresponding author e-mail: mpg14@psu.edu

Abstract

Current projections of the oceanic response to anthropogenic climate forcings are uncertain. Two key sources of these uncertainties are (i) structural errors in current Earth system models and (ii) imperfect knowledge of model parameters. Ocean tracers observations have the potential to reduce these uncertainties. Previous studies typically consider each tracer separately, neglect potentially important statistical properties of the system, or use methods that impose rather daunting computational demands. Here we extend and improve upon a recently developed approach using horizontally averaged vertical profiles of chlorofluorocarbon (CFC-11), radiocarbon (Δ^{14}C), and temperature (T) observations to reduce model parametric and structural uncertainties. Our method estimates a joint probability density function, which considers cross-tracer correlations and spatial autocorrelations of the errors. We illustrate this method by estimating two model parameters related to the vertical diffusivity, the background vertical diffusivity and the upper Southern Ocean mixing. We show that enhancing the upper Southern Ocean mixing in the model improves the representations of ocean tracers, as well as improves hindcasts of the Atlantic Meridional Overturning Circulation (AMOC). The most probable value of the background vertical diffusivity in the pelagic pycnocline is between 0.1-0.2 cm^{2}s^{-1}.

———

According to the statistical method, observations of Δ^{14}C reduce the uncertainty about the background vertical diffusivity the most followed by CFC-11 and T. Using all three tracers jointly reduces the model uncertainty by 40%, more than each tracer individually. Given several important caveats, we illustrate how the reduced model parametric uncertainty improves probabilistic projections of the AMOC.

1. Introduction

The North Atlantic Overturning Circulation (AMOC) is a key component of the climate system [*Munk & Wunsch*, 1998]. Past changes in the AMOC intensity are associated with considerable changes in global scale temperature and precipitation patterns [*McManus et al.*, 2004]. Anthropogenic climate forcings may trigger an AMOC threshold response, with potentially serious impacts on natural systems and human welfare [*Patwardhan*, 2007; *Keller et al.*, 2000]. Current AMOC model predictions are deeply uncertain [*Zickfeld et al.*, 2007; *Meehl et al.*, 2007].

Tracer observations such as chlorofluorocarbon-11 (CFC-11) and radiocarbon ($\Delta^{14}C$) provide information on the ventilation rate and advective properties in the ocean on time-scales ranging from decadal to centennial that can be used for evaluating the skill of climate models in simulating the ocean circulation [*Doney et al.*, 2004]. A better representation of these processes in models can possibly improve AMOC projections.

A key variable for determining ocean circulation properties in models is the vertical ocean diffusivity (K_v). Changing this value in model simulations has a large impact on oceanic heat storage and transport, uptake of ocean tracers such as CO_2 [*Sokolov et al.*, 1998], and on the work necessary to lift the abyssal waters through stratification (that closes the MOC circulation) [*Wunsch & Ferrari*, 2004]. This variable is highly uncertain [*Munk & Wunsch*, 1998], and it is sometimes tuned in models to generate a realistic AMOC strength [*Gao et al.*, 2003]. In addition, this parameter value affects the existence of multiple states of the MOC in model simulations [*Schmittner & Weaver*, 2001].

Various processes lead to mixing in the ocean such as shear or buoyancy forced turbulence, interactions of flow with topography, and double diffusion (differential molecular diffusion of heat and salt). See *Smyth & Moum* [2001] and *Moum & Smyth* [2001] for reviews. Although General Circulation Models have been increasing their ability of parameterizing subgrid scale turbulent processes in the ocean (*Bryan & Lewis* [1979]; *Pacanowski & Philander* [1981]; *Large et al.* [1994]; *Ferrari et al.* [2008]), due to the complexity of the problem and processes involved, most schemes are still highly simplified and parameterized. In Earth System Models of Intermediate Complexity (EMICs), the absence of more complex parameterizations elevates the importance of the parameters related to K_v in order to fulfill the model necessity of turbulent mixing in simulating a realistic AMOC strength.

Several studies [e.g. *England*, 1993; *Gao et al.*, 2003] analyze the importance of the magnitude of the diffusivity strength and parameterization on the MOC structure and representations of tracers in ocean models. These studies are typically silent on the question of how much information is contained in the different types of observations. This is an important question, for example, to inform the design of AMOC observation and prediction systems [cf. *Baehr et al.*, 2008; *Keller et al.*, 2007].

Schmittner et al. [2009] discusses a relatively simple but computationally efficient method to estimate the background ocean diffusivity K_{bg} from the combination of spatially resolved ocean tracer observations considering both, observational and model errors. However, *Schmittner et al.* [2009] neglects the effects of cross-correlation between different tracers, which limits the number of tracers that can be combined in a joined probability density function. In another recent study, *Bhat et al.* [2009] estimates the posterior prob-

ability distribution for K_{bg} using Δ^{14}C and CFC-11 observations. Their approach uses a

Gaussian process emulator for the climate model and estimates the distribution of K_{bg}

via a Bayesian approach. While their kernel mixing based approach to constructing the

emulator is flexible and efficient, it is conceptually complex and computationally highly

demanding for routine use with more than two ocean tracers.

Here we estimate the probability density function (pdf) of K_{bg} using three tracers si-

multaneously. Our approach provides a fast and easy way to implement the methodology,

enabling the routine use of information from several ocean tracers jointly, while still con-

sidering spatial autocorrelation as well as cross-correlation between residuals of different

tracers. We demonstrate how neglecting cross-correlation and/or simplifying the mean

function can compromise the accuracy of the estimation. We improve the treatment of

uncertainties surrounding K_v in the model by considering the structural uncertainty about

the upper Southern Ocean mixing (u_K_{SO}). We show that an ensemble with enhanced

Southern Ocean mixing is more consistent with the observations.

Furthermore, we advance on previous work by quantifying and ranking the skill of the

tracers CFC-11, Δ^{14}C and temperature (T) to constrain the uncertainties in the model

parameter K_{bg}. We demonstrate the potential utility of the considered observations to

improve model predictions of the AMOC.

2. Methods

2.1. Earth System Model of Intermediate Complexity

We use the University of Victoria Earth System Model of Intermediate Complexity

(UVic 2.8; *Weaver et al.* [2001]). This model has been widely used in climate simulations

and models comparisons studies. In the UVic model, we parameterize the diapycnal

diffusivity as $K_v = K_{tidal} + K_{SO} + K_{bg}$, which consists of the diffusivity due to local

dissipation of tidal energy and its resulting generation of turbulence and mixing (K_{tidal},

Simmons et al. [2004]), a parametrization for the vigorous mixing (K_{SO}) observed in the

Southern Ocean [e.g. *Naveira Garabato et al.*, 2004], plus a background diffusivity K_{bg}

that represents all other processes that lead to mixing, such as non-local dissipation of

tidal energy, mesoscale eddy activity, double diffusion, hurricanes, interaction of flow with

topography, and others.

The model accounts for increased mixing over rough topography based on the tidal

mixing scheme of *St. Laurent et al.* [2002], and uses the *Gent & McWilliams* [1990]

eddy mixing parameterization. It is likely that K_{bg} is spatially and temporally variable

in nature [*Sriver et al.*, 2010], but due to a lack of a more explicit representation of the

processes and for simplicity we assume a constant value of K_{bg} everywhere. Note that

K_{tidal} decays exponentially (with an e-folding depth of 500 m above the sea floor) such that

it is unimportant in the pelagic pycnocline (i.e., away from the boundaries). However,

it is the value of K_{bg} in the pelagic pycnocline that is most important in determining

the large scale ocean circulation in models [c.f., *Marotzke*, 1997; *Munk & Wunsch*, 1998].

For the Southern Ocean (south of 40S) parametrization, the vertical mixing is truncated

at 1 cm^2/s as a lower bound ($K_v > 1$ cm^2/s). The Southern Ocean is one of the most

tempestuous oceans on earth, and these transient effects may produce strong turbulent

mixing, specially in the upper Southern Ocean. In order to include uncertainties about the

upper Southern Ocean mixing, we further divide the Southern Ocean mixing into upper

(u_K_{SO}) and lower (l_K_{SO}) parts. Therefore, $K_{SO} = u\_K_{SO} + l\_K_{SO}$, where u_K_{SO} is the

Southern Ocean mixing in the upper 500 m, and l_K_{SO} is the Southern Ocean mixing

from 500m to the bottom of the water column.

We create two ensembles to analyze the uncertainty in two model parameters, the

background ocean diffusivity (K_{bg}) and the upper Southern Ocean diffusivity (u_K_{SO}).

Each ensemble contains seven members, corresponding to a grid of the parameter K_{bg}

values of (0.05, 0.1, 0.15, 0.2, 0.3, 0.4, and 0.5) cm^{2}s^{-1}. The difference between the two

ensembles is that in the first one (ENSEMBLE 1), the enhanced SO mixing is only applied

in the lower part of the Southern Ocean, so in the upper SO the mixing is equal to the

rest of the pelagic areas of the upper ocean (with indices u_K_{SO}=0, l_K_{SO}=1), whereas

the second one (ENSEMBLE 2) uses an enhanced mixing in the entire column of the

Southern Ocean (with indices u_K_{SO}=1, l_K_{SO}=1). As we are not varying the parameter

l_K_{SO}, it is suppressed in the rest of the manuscript.

The ocean component in UVic is MOM2 [*Pacanowski*, 1995] with a $1.8° \times 3.6°$ reso-

lution in the horizontal and 19 depth levels. The atmospheric component is a one-layer

atmospheric energy-moisture balance model, which does not apply flux correction and

is forced by prescribed winds from the NCAR/NCEP climatology. Also included in the

model are a thermodynamic sea-ice component, a terrestrial vegetation (TRIFFID), and

an oceanic biogeochemistry based on the ecosystem model of *Schmittner et al.* [2005].

A total of 47,600 model years was preformed, what makes UVic suitable for this kind

of study. At first, the model is spun up from observed data fields as initial conditions

for 3000 years (with a coupled carbon cycle for the last 1000 years) for each parameter

value. It is then integrated from years 1800-2100 using historical and projected climate

forcings (SRES–A1FI scenario), extended to the year 2200 following *Zickfeld et al.* [2008].

132 We modify the model to include non-CO_2 greenhouse gases, volcanic and sulfate forcings

133 from *Sato et al.* [1993] and *Hansen & Sato* [2004]. Atmospheric sulfates data enter the

134 model as gridded optical depth [*Koch et al.*, 1999], and follow the same rate of decrease

135 as the CO_2 concentration after 2100.

2.2. Data

136 We focus on a subset of observations that have previously been shown to provide con-

137 straints on the parameterization of K_v in ocean models: (i) temperature (T), (ii) chlo-

138 rofluorocarbon 11 (CFC-11), and (iii) radiocarbon ($\Delta^{14}C$) observations [cf. *Schmittner*

139 *et al.*, 2009; *Bhat et al.*, 2009; *Toggweiler et al.*, 1989]. $\Delta^{14}C$ is defined as the $^{14}C/^{12}C$

140 ratio of air-sea fractionation-corrected data [*Stuiver & Polach*, 1977]. Each of the trac-

141 ers in this subset has a different behavior, and can constrain K_v in different ways. The

142 temperature observations constrain K_v, because K_v affects, for example, the shape of the

143 thermocline as well as the penetration of the anthropogenic heat anomalies [*Gnanade-*

144 *sikan*, 1999]. The $\Delta^{14}C$ observations can constrain K_v in two main ways, because it has

145 a natural and an anthropogenic component. The natural component can provide infor-

146 mation of mixing rates (that are, in turn, a function of K_v) in the order of centuries or

147 millennia. The anthropogenic component, which greatly increased during the 1950s and

148 1960s due to thermonuclear explosions, provides information on decadal time-scale. Here

149 we do not make distinction between natural and bomb 14C, thus we use its total con-

150 centration. The anthropogenic tracer CFC-11 also constrains K_v on decadal time-scale,

151 because atmospheric emissions started in the 1930s. The solubility of CFCs in water is

152 dependent on the temperature. Considering CFC-11 and $\Delta^{14}C$ jointly can provide new

153 insights into vertical oceanic mixing because they have very different forcing histories,

air-sea equilibration timescales and water solubility [*Broecker & Peng*, 1974; *Ito et al.*,

2004], and the observation errors and signal-to-noise ratios of the two tracers are different.

We analyze published data products for these three tracers [*Locarnini et al.*, 2006; *Key et*

al., 2004] and average the model hindcasts over the time the observations have been col-

lected, i.e., 1990's for CFC-11 and Δ^{14}C, and 1950-2000 for temperature. We interpolate

the observations to the model grid and the model output is restricted to the regions where

the data products are available. All considered ocean tracer observations are horizontally

averaged into global mean vertical profiles. Further, the probability distributions of the

model parameters, inferred from the information of ocean tracers profiles, are compared

with the distribution inferred from the climatological observations of the AMOC strength

at 24°N. For this purpose, we use the information of the AMOC strength calculated with

the inverse model of *Lumpkin & Speer* [2003], which is estimated as (17.6±2.7 Sv). The

model ensembles are calibrated against observations using a Bayesian inference method.

We assume a Gaussian likelihood function and estimate the posterior probability of K_{bg}

and u_K_{SO} given the observations through a Markov Chain Monte Carlo (MCMC) method

[*Metropolis et al.*, 1953]. Our method accounts for auto-correlations of the residuals, as

well as cross-correlation between residuals of different tracers. For this, a separable co-

variance matrix Σ is estimated. The inversion and the numerical implementation of the

calibration procedure are detailed in the next subsection. Readers not interested in the

details of the statistical inversion technique can skip the next subsection without loss of

understanding.

2.3. Bayesian model inversion

175   The goal of Bayesian parameter estimation is to infer a probability distribution(s) $p(\theta|O)$

176   representing the uncertainty in one (or more) climate model parameter θ, conditional on a

177   vector of observed data O. Here θ are parameters K_{bg} and u_K_{SO}, which are related to the

178   vertical ocean diffusivity in UVic. The inferential procedure is based on a statistical model

179   that relates the model parameters (θ) to the observations (O) by way of the ensemble of

180   model output $M(\theta)$. The statistical model used here assumes that the observations are

181   randomly distributed around the model prediction, according to

$$O = M(\theta) + \epsilon, \tag{1}$$

182   where the error is a random variable drawn from a multivariate normal distribution

$$\epsilon \sim N(\mu, \Sigma), \tag{2}$$

183   with an unknown mean or bias term μ and covariance matrix Σ. These distributional

184   parameters are estimated along with the model parameter θ. The error term encompasses

185   all processes which may cause the observations to deviate from the model predictions,

186   including model structural error, unresolved variability in the climate system, and mea-

187   surement error. We model these errors as random processes, approximated here by a

188   potentially correlated Gaussian probability function.

189   The error mean term μ represents model bias, which is common for each observed

190   variable across ensemble members. *Schmittner et al.* [2009] assumed a bias which is

191   constant with depth. Here we expand upon this form by using a general linear form that

192   varies with depth (z), $\mu = az + b$. This form improves the model fit as indicated by

a exploratory data analysis in the next section. The covariance matrix, described later,

captures the residual variability that is unaccounted by the linear bias term.

The above probability model describing the spread of observations about the model

output defines a likelihood function $L(O|\theta, \mu, \Sigma)$ for the data conditional on the model

and covariance parameters:

$$L(O|\theta, \mu, \Sigma) = (2\pi)^{-N/2}|\Sigma|^{-1/2} \exp\left(-\frac{1}{2}\tilde{r}^T \Sigma^{-1} \tilde{r}\right) , \tag{3}$$

where Σ is a covariance matrix and $\tilde{r} = O - M(\theta) - \mu$ are the bias-corrected data-model

residuals.

Consider an ensemble M containing p runs of a climate model, where each run corre-

sponds to a different value of a climate model parameter, θ_k, $k = 1, \ldots, p$. For each ensem-

ble member we analyze n ocean tracer profiles defined at d spatial locations (depths). The

matrix Σ is $nd \times nd$ specifying the covariance between n tracers at d locations (depths).

Assuming separability, Σ can be approximated by a Kronecker product of two matrices:

$$\Sigma = \Sigma_T \otimes C_S + \Sigma_M , \tag{4}$$

where Σ_T corresponds to the $n \times n$ cross-covariance matrix of the tracers, and C_S is

the $d \times d$ spatial correlation matrix (in depth) respectively. Σ_M is the data measurement

error which we assume to be negligible compared to the other errors because of the spatial

aggregation of the data.

The cross-covariance matrix Σ_T depends on $n(n-1)/2$ cross-tracer correlation coef-

ficients ρ_{ij} (since $\rho_{ij} = \rho_{ji}$), and on residual standard deviations σ_i of the n individual

tracers:

$$\Sigma_T = \begin{bmatrix} \sigma_1^2 & \sigma_1\sigma_2\rho_{12} & \dots & \sigma_1\sigma_n\rho_{1n} \\ \sigma_2\sigma_1\rho_{21} & \sigma_2^2 & \dots & \sigma_2\sigma_n\rho_{2n} \\ \vdots & \vdots & \ddots & \vdots \\ \sigma_n\sigma_1\rho_{n1} & \dots & \dots & \sigma_n^2 \end{bmatrix} . \tag{5}$$

We model the spatial correlation C_S using a Gaussian correlation function, a special case of the Matérn class of covariance functions (see, for e.g., *Stein* [1999]). This function decays with distance between locations d_i and d_j with a correlation length scale λ, assumed to be the same for all tracers:

$$(C_S)_{ij} = \exp\left(-\frac{|d_i - d_j|^2}{\lambda^2}\right) . \tag{6}$$

Given the property of the Kronecker product (see, for example, *Lu & Zimmerman* [2005]), the multivariate normal likelihood function $L(y, \theta)$ becomes:

$$L(O|\theta, \mu, \Sigma_T, C_S) = (2\pi)^{-N/2}(|\Sigma_T|^d|C_S|^n)^{-1/2}\exp\left[-\frac{1}{2}\tilde{r}^T(\Sigma_T^{-1} \otimes C_S^{-1})\tilde{r}\right] , \tag{7}$$

where $N = nd$ is the total number of data points, and $\tilde{r} = [O_1 - M_1 - \mu_1, \dots, O_n - M_n - \mu_n]^T$ is the concatenated vector containing the misfit between the unbiased model predictions and the corresponding observations for the considered tracers. The Kronecker structure of Equation 4 allows the $nd \times nd$ matrix Σ to be efficiently inverted by inverting the two smaller matrices Σ_T ($n \times n$) and C_S ($d \times d$).

Once the probability model has been specified in the form of a likelihood function, the Bayes' theorem allows inference about the posterior distribution of θ. The theorem states that the posterior probability of the unknown parameters is proportional to their prior probability distribution, multiplied by the likelihood of the data, according to:

$$p(\theta, a, b, \sigma, \rho, \lambda | O) \propto L(O | \theta, a, b, \sigma, \rho, \lambda)\, p(\theta)\, p(a)\, p(b)\, p(\sigma)\, p(\rho)\, p(\lambda)\,. \qquad (8)$$

We draw 20,000 samples from the above posterior distribution by a Markov chain Monte Carlo (MCMC) algorithm. The MCMC algorithm jointly estimates the model parameters ($\theta = K_{bg}, u\_K_{SO}$), $2n$ bias coefficients (a_i and b_i), n standard deviations (σ_i), $n(n-1)/2$ cross-tracer correlations (ρ_{ij}), and one correlation length (λ). This is an improvement upon the methodology of *Schmittner et al.* [2009] which held all parameters but θ fixed at optimized values, and did not consider the uncertainty in the other parameters. Because the model output is only defined on a discrete grid of values, the MCMC algorithm proposes discrete jumps for the parameters θ during its random walk through parameter space, and continuous moves for all other parameters.

We choose a uniform prior $p(\theta)$ for the model parameters K_{bg} and u_K_{SO}. For the correlation length we apply the lognormal prior $\ln \lambda \sim N(5.5, 0.5^2)$, such that the logarithm of λ is normally distributed with mean 5.5 and standard deviation 0.5. This prior locates most of the probability mass of the distribution between 0 and 600 meters. We use normal priors for the bias parameters a_i and b_i, p(a_i)=N(0,($\sigma_i/\lambda)^2$) and p(b_i)=N(0,σ_i^2). For the estimate of individual tracers distributions, where the cross-correlation matrix is a scalar (i.e. $\Sigma = \sigma_1^2$), we use a Jeffreys prior ($p(\sigma_i) \propto 1/\Sigma$). When the multi-tracer cross-covariance matrix is estimated, we specify an inverse Wishart prior distribution $\Sigma_T \sim IW(S, \nu)$, with a diagonal scale matrix $S = I$ and $\nu = 2n + 1$ degrees of freedom. A diagonal scale matrix reduces spurious correlations by penalizing tracer residuals which are not independent of each other. Spurious correlation is not a problem when the data dimension is large, but when the data are sparse such a regularization procedure is pru-

248 dent (see, for instance, *Barnard et al.* [2000] or Chapter 19 in *Gelman et al.* [2003], and

249 references therein).

Equation (8) provides the joint posterior probability of both the model parameter and

the bias and covariance parameters. The marginal posterior probability of the model

parameter alone is obtained by integrating the joint posterior over all other parameters:

$$p(\theta|O) = \int p(\theta, a, b, \sigma, \rho, \lambda|O) \, da \, db \, d\sigma \, d\rho \, d\lambda \,. \tag{9}$$

250 Since the posterior is estimated by MCMC sampling, this posterior distribution of θ is

251 easily obtained by simply considering the θ samples while ignoring the samples for the

252 other parameters.

3. Results

3.1. Effect of ocean diapynal diffusivity on the AMOC hindcasts and spatial fields

253 In the adopted model the AMOC strength is positively correlated with the parameters

254 K_{bg} and u_K_{SO} (Figure 1). K_{bg} has a strong influence on the model hindcasts of the

255 maximum AMOC strength, while the AMOC sensitivity to u_K_{SO} is weaker. The range

256 of AMOC strength varies from about 5–23 Sv across all simulations. The inclusion of

257 enhanced upper Southern Ocean mixing ($u\_K_{SO} = 1$), can increase the AMOC by a few

258 Sverdrups, with more influence at lower K_{bg}. Under the projected climate forcings, the

259 AMOC strength decreases in most cases, but it is more sensitive (in absolute values) to

260 the considered forcings for higher diffusivity values. Due to the strong dependence of the

261 AMOC structure and behavior on the values of the parameters K_{bg} and u_K_{SO} in this

262 model, a reduction in the parametric uncertainty has the potential to improve AMOC

263 hindcast and projection in the model.

²⁶⁴   The different parameter values result in different hindcasts of ocean tracers such as CFC-

²⁶⁵ 11 (Figure 2) and Δ^{14}C (Figure 3), due to the different tracers advection and diffusion rates

²⁶⁶ in the model. Higher K_{bg} values result in stronger vertical water exchange, increased deep

²⁶⁷ water mass formation, which carries water with higher tracer content from the surface, and

²⁶⁸ decreased vertical stratification in the ocean. u_K_{SO} broadly produces the same effects

²⁶⁹ of K_{bg}. Nevertheless, u_K_{SO} impacts more heavily the lower K_{bg} runs and the Southern

²⁷⁰ Ocean stratification.

²⁷¹   Here we analyze the tracers concentrations as vertical profiles of their averaged con-

²⁷² centrations over the globe. We consider three different observations, CFC-11, $\Delta^{14}C$ and

²⁷³ T (Figure 4, shown as an example for ENSEMBLE 1). In general, the observations are

²⁷⁴ contained by the model ensemble spread, except for T in the deep ocean, which is too

²⁷⁵ cold in the model.

3.2. The uncertainty of the statistical inversion

²⁷⁶   The inversion method uses the information contained in the tracers to estimate the

²⁷⁷ model parameter K_{bg}, taking into account uncertainties in u_K_{SO}. Key improvements

²⁷⁸ compared to *Schmittner et al.* [2009] are: (i) the estimation of the cross-correlation terms;

²⁷⁹ (ii) a more refined representation of structured biases in the Likelihood function; and

²⁸⁰ (iii) the consideration of the effects of the structural uncertainty (specifically about the

²⁸¹ implementation of mixing in the SO). Here we demonstrate how these improvements affect

²⁸² the joint posterior pdf of the model parameters. We test the sensitivity of the method to

²⁸³ the choice of the statistical (or nuisance) parameters for the distribution of K_{bg}. In this

²⁸⁴ sensitivity test, we do not account for uncertainties in the parameter u_K_{SO}. Therefore,

²⁸⁵ we only use outputs from ENSEMBLE 1.

For illustration, we use two tracers, $\Delta^{14}C$ and T, as input for the statistical inversion. We calculate four inversion, which vary the number of statistical parameters to be estimated. The structure of the errors differ from each other by the representation of two main parameters, the bias and the cross-correlation of the residuals between the model and the observations. The bias term represents our guess of the mean function of the residuals. We demonstrate the trade-off between complexity of the bias-correction and the covariance structure of the residuals in this simple sensitivity study.

Specifically, we analyze four different assumptions about the structural error terms. First, we use a simple case where the bias is constant and there is no residuals cross-correlation; second, we use a constant bias and estimate the cross-correlation; third we estimate a linear bias but no residual cross-correlation; and fourth, in which linear bias and cross-correlation are both estimated. To summarize the experiments in the sensitivity study, we have: a) $\mu = b$, $\rho =0$, b) $\mu = b$, $\rho = \hat{\rho}$, c) $\mu = az + b$, $\rho =0$, and d) $\mu = az + b$, $\rho = \hat{\rho}$. Note that the calibration also estimates standard deviation, correlation length and the model parameter, as described in Section 2.3. Comparing all pdfs (Figure 5) we see that for the individual pdfs the representation of the bias term can be essential for the model parameter estimation. When a more simplified bias ($\mu = b$) is applied (Figures 5a and 5b), the pdfs in this example are displaced toward higher K_{bg} values, and centered on 0.3 and 0.4 $cm^2 s^{-1}$. In contrast, with the linear bias estimations, the mode of K_{bg} pdf is centered around 0.15 and 0.2 $cm^2 s^{-1}$. For the cases with linear bias (cases c and d), the standard deviation of the residuals of both tracers (Table 1) decrease in comparison to the constant biases cases (cases a and b). On the other hand, the standard deviations of the residuals are not influenced by the addition of cross-correlation parameters.

The inclusion of the cross-correlation parameter impacts the position of the joint posterior (black curves), and its strength is closely related to the representation of the bias. When the bias has a better representation, which is the linear bias case here (Figures 5c and 5d), the cross-correlation term has little influence on the joint pdf. A comparison of the strength of the cross-correlation parameters (cases (b) and (d) in Table 1) shows that $\rho = 0.70$ when μ is constant, and is much smaller $\rho = 0.40$ when μ is linear. Comparing the posteriors of the cases (a) and (b) (Figures 5a and 5b), ρ can visibly change the posterior when the mean function is less structured. Case (b) shows a counterintuitive result where the posterior mode is distant from the modes of the individual components (Figure 5b). This result indicates that with a relatively poor representation of the mean (bias) function, considering or neglecting the effects of this residual cross-correlation can drastically change the K_{bg} posterior estimate. This effect becomes less pronounced, as the representation of the model bias term improves (eg. Figure 5b vs. Figure 5c). As discussed by *Cressie* [1993] (pp. 25), "What is one person's (spatial) covariance structure may be another person's mean structure". In other words, there is a trade-off between estimating a mean function for the tracer residuals to account for structural model errors and the magnitude of the residual cross correlation across the considered sources of information.

3.3. Estimating the uncertainty of vertical diffusivity

The analysis so far illustrates how different tracers observations can be combined to reduce uncertainty about one mixing parameter (K_{bg}). This reduction in parametric uncertainty results, at least in the framework of the adopted model, in a reduction of the prediction uncertainty about the AMOC. Of course, there are several caveats associated

with structural errors and other neglected uncertainties in this study. We return to this

issue in the Section 4, below. In this section we illustrate how this information can

potentially be used to reduce uncertainties in two model parameters and improve model

hindcasts and projections of the AMOC. Here the inversion uses our best estimate of

the model bias term (linear), and accounts for cross-tracer correlation. We make three

inversions (Figure 6), one to estimate K_{bg} for the ENSEMBLE 1, a second to estimate K_{bg}

for the ENSEMBLE 2, and a third inversion which uses information from both ensembles

to generate probability distributions for K_{bg} and u_K_{SO} in a Bayesian model average

fashion.

Information from the three considered tracers, CFC-11, T and $\Delta^{14}C$, is introduced in

the statistical inversion for the estimation of uncertainties in the model parameters. For

comparison, we also show in Figure 6 the K_{bg} pdf obtained using the climatological AMOC

observations. The K_{bg} pdf is derived from estimate of the climatological AMOC strength

of *Lumpkin & Speer* [2003] by assimilating a single data point assuming a normally dis-

tributed error. In principle, the model could be calibrated with both the ocean tracers and

AMOC strength data by using the derived AMOC pdf as a prior for K_{bg}. However, this

would neglect potential correlations between ocean tracer and AMOC strength residual

errors. As a proper treatment of AMOC/tracer correlations is beyond the scope of this

work, we present the AMOC-derived pdf just for comparison, without assimilating it in

the joint posterior pdf.

The tracers distributions of both ensembles show similar behavior. Nevertheless, the

ENSEMBLE 1 (Figure 6a) has in general higher K_{bg} modes in comparison to ENSEMBLE

2 (Figure 6b). This result shows that the additional mixing over the upper Southern Ocean

increases the overall magnitude of K_v, without changing K_{bg}, and tends to intensify the AMOC. The posterior pdf for K_{bg}, obtained by assimilating observations of the AMOC strength only (lines with triangles), is also displaced to lower values in ENSEMBLE 2, because ENSEMBLE 2 has stronger AMOC values for the same K_{bg} (Figure 1)

When information from both ensembles are added together (Figures 6c and 6d), the ENSEMBLE 2 dominates the Markov chain for $\Delta^{14}C$ and T, with probabilities of 100 % and 65 % for ENSEMBLE 2, respectively. Conversely, CFC-11 has 80% probability of happening ENSEMBLE 1 (Figure 6d). The joint posterior of all tracers encompassing the two ensembles (Figure 6c) is entirely described by ENSEMBLE 2, therefore the posteriors in Figures 6b and 6c are practically identical.

When all the two model parameters are assimilated jointly (Figure 6c), the considered sources of information have rather different skill in improving K_{bg} estimates and AMOC predictions (see Table 2 for the properties of the statistical distributions). Δ^{14}C has the highest information content with respect to improving K_{bg} estimates, its posterior 95 % credible interval (CI) is the tightest (0.21 cm^{2}s^{-1}) in comparison to the other tracers. CFC-11 comes in second, with a 95 % CI of 0.24 cm^{2}s^{-1}, and T comes last with the largest CI of 0.26 cm^{2}s^{-1}.

Combining the information of the three considered tracers (line with squares in Figure 6c), favors K_{bg} values in the lower part of the considered range, from 0.1–0.2 cm^{2}s^{-1}. Note that the joined probability density function is narrower than each individual pdf indicating an advantage of using multiple tracer observations in reducing the parameter uncertainty.

376   As discussed in previous studies [e.g. *Schmittner et al.*, 2009], the K_{bg} value in a coarse

377   resolution ocean model represents the effects of background diffusivity combined with

378   subgridscale diffusivity (i.e., a model shortcoming). Another shotcoming for coarse z-

379   coordinate ocean models is the numerical diffusivity (Veronis effect), which can generate

380   spurious diapycnal diffusion, especially in long climate simulations, in western boundary

381   regions and regions where the isoneutral slope is large [*Griffies et al.*, 1998, 2000]. Hence,

382   even if our model-based estimate does not represent directly the observational estimate of

383   pelagic diffusivity of 0.1 cm^{2}s^{-1} [*Ledwell et al.*, 1993], they appear to be more consistent

384   when we improve on the parametrization of regional mixing in the model.

3.4. AMOC projections

385   The joint posterior K_{bg} and u_K_{SO} estimates (Figures 6c and 6d) can be used to derive

386   model projections of the AMOC in 2100 and 2200 (Figure 7). The model hindcast for the

387   maximum AMOC strength in 2000 is about 15–15.5 Sv. In 2100, the expected strength for

388   the AMOC in this model is about 11 Sv. In 2200 the AMOC shows a slight strengthening

389   relative to the 2100 conditions with an expected value of roughly 12 Sv.

390   The K_{bg} and u_K_{SO} estimates suggest an AMOC hindcast for the year 2000 (Figure 7)

391   that is about 2 Sv weaker than the climatological AMOC estimates of *Lumpkin & Speer*

392   [2003]. The inclusion of the parameter u_K_{SO} in the analysis reduces significantly the

393   discrepancy of the AMOC estimates relative to the K_{bg} (Figure 6c). Other systematic

394   model bias(es), such as too weak buoyancy forcing (e.g. from errors in the simulation

395   of the atmospheric hydrological cycle and surface freshwater fluxes) can compromise the

396   estimates of the current and projected AMOC strength for the Uvic model. Further

397   discussion and implications are described in the next section.

4. Caveats

Our results are subject to many caveats. These caveats point to potentially fruitful research directions. In the statistical part, we consider only highly aggregated data. Basinwide zonal averages could, for example, provide potentially useful information on where the model performs better. In the projection part, other model parameters, such as those affecting the response of the ocean-atmosphere coupled system, for example, the hydrological cycle [*Saenko & Weaver*, 2004], climate sensitivity or sensitivity of climate to aerosol concentrations, [cf. *Tomassini et al.*, 2007; *Forest et al.*, 2002], are also highly uncertain, and can impact (probably widen) probabilistic AMOC projections and should be considered. In addition, the atmospheric model in UVic is rather simplified, and neglects important ocean-atmosphere feedbacks.

UVic does not use flux correction. Freshwater flux correction is known to improve the salinity and stratification in ocean models [*Sorensen et al.*, 2001], and can be used to improve projections and hindcasts.

In the hindcasts part, other parameters linked to both diapycnal and isopycnal mixing may affect the structure of the AMOC. Nevertheless, according to *Jayne* [2009], tidal mixing parameters in the *St. Laurent et al.* [2002] parameterization have relatively low impact on the strength of the AMOC, and that upper-ocean wind-driven mixing may have a much stronger impact.

We show how including regional aspects of vertical mixing can improve the representation of the AMOC. The model parameters uncertainties need to be estimated together as performed here, since addition of new parameters can change the structure of the other calibrations. *Jayne* [2009] describes, "this is the typical conundrum: it is difficult to as-

420 sess whether any of the given parameterizations improve the model since comparing to

421 observational metrics may obscure compensating errors in different parameterizations".

5. Conclusion

422 We develop and apply a computationally efficient and statistically sound method to

423 rank and quantify the skill of different sources of information to reduce the uncertainty

424 about ocean model parameters and the resulting climate predictions. We improve on

425 previous work by (i) refining the estimation of errors in the model structure, (ii) including

426 several ocean tracers and two model parameters at once in a computationally efficient

427 fashion, and (iii) quantifying and ranking the skill of different sources of information to

428 reduce the uncertainty about a model parameter. Subject to the aforementioned caveats,

429 we show how Δ^{14}C, CFC-11, and T together sharpen the estimates of K_{bg} by 40 % and

430 improve AMOC projections in the UVic model.

431 The K_{bg} derived from individual observations (i.e., Δ^{14}C, CFC-11, T) are broadly con-

432 sistent, but show slight discrepancies that we attribute predominantly to structural model

433 errors. Of the considered observations, Δ^{14}C has the highest skill in reducing uncertainties

434 in AMOC projections, but it is also the most distant from the pdf observational derived

435 AMOC estimates. $\Delta^{14}C$ is followed (in decreasing skill of being able to reduce K_{bg} uncer-

436 tainty) by CFC-11 and T. The second parameter analyzed in this work, u_K_{SO} improved

437 the representations of C14 and T in the model, and improves the representation of the

438 AMOC strength.

439 AMOC projections show a reduction of the maximum of the joint posterior in 2100

440 by roughly 25% (3.5 Sv). Perhaps both surprisingly and encouraging, the pdfs of K_{bg}

441 estimated in this study are quite similar among the considered ocean tracers and the two

ensembles analyzed, which have different different representations of the upper Southern Ocean mixing and AMOC. This convergence of K_{bg} estimates based on different sources of information and parameterizations suggest that K_{bg} can be robustly estimated from the oceanic tracers studied here.

References

Baehr, J., D. McInerney, K. Keller, and J. Marotzke (2008), Optimization of an observing system design for the North Atlantic meridional overturning circulation, *J. of Atmos. and Ocean. Tech.*, **25**, 625–634.

Barnard, J., R. McCulloch and X. Meng (2000), Modeling covariance matrices in terms of standard deviations and correlations with application to shrinkage, *Statistica Sinica*, **10**, 1281–1311.

Bhat, K.S., Haran, M., Tonkonojenkov, R., and Keller, K. (2009), Inferring likelihoods and climate system characteristics from climate models and multiple tracers. Technical report, Department of Statistics, Penn State University, USA.

Broecker, W.S., and T.H. Peng (1987), Gas exchange rates between air and sea. *Tellus*, **26**, 21–35.

Bryan, K., and L.J. Lewis (1979), A water mass model of the world ocean. *J. Geophys. Res.*, **84**(C5), 2503–2517.

Bryan, F. O., G. Danabasoglu, P. R. Gent, and K. Lindsay (2006), Changes in ocean ventilation during the 21st century in the CCSM3. *Ocean Model.*, **15**, 141–156.

Cressie, N.A. (1993), Statistics for Spatial Data, Wiley, New York, 900 pp.

Dalan, F., P.H. Stone, and A.P. Sokolov (2005), Sensitivity of the Oceans Climate to Diapycnal Diffusivity in an EMIC. Part II: Global Warming Scenario. *J. Climate*, **18**, 24822496.

Danabasoglu, G., J. C. McWilliams, and P. R. Gent (1994), The role of mesoscale tracer transports in the global ocean circulation. *Science*, **264**, 1123–1126.

Doney et al. (2004), Evaluating global ocean carbon models: The importance of realistic physics. *Glob. Biogeochem. Cycles*, **18**, GB3017, doi:10.1029/2003GB002150.

England, M. H. (1993), Representing the global-scale water masses in ocean general circulation models. *J. Phys. Oceanogr.*, **23**, 1523–1552.

Ferrari, R., J. C. McWilliams, V. M. Canuto, M. Dubovikov (2008), Parameterization of eddy fluxes near oceanic boundaries. *J. Climate*, 21, 2770-2789,doi:10.1175/2007JCLI1510.1.

Chris E. Forest, Peter H. Stone, Andrei P. Sokolov, Myles R. Allen, and Mort D. Webster (2002), Quantifying Uncertainties in Climate System Properties with the Use of Recent Climate Observations. *Science*, **295** (5552), 113. [DOI: 10.1126/science.1064419].

Gao, Y., H. Drange, and M. Bentsen (2003), Effects of diapycnal and isopycnal mixing on the ventilation of CFCs in the North Atlantic in an isopycnic coordinate OGCM. *Tellus*, **55B**, 837–854.

Gelman, A., J.B. Carlin, H. S. Stern, and D. B. Rubin (2003), Bayesian Data Analysis, second edition. London: CRC Press.

Gent, P. R., and J. C. McWilliams (1990), Isopycnal mixing in ocean circulation models. *J. Phys. Oceanogr.*, **20**, 150–155.

Gent, P. R., F. O. Bryan, G. Danabasoglu, K. Lindsay, D. Tsumune, M. W, Hecht, and S. C. Doney (2006), Ocean Chlorofluorocarbon and Heat Uptake during the Twentieth Century in the CCSM3. *J. Climate*, **19**, 2366–2381.

Gnanadesikan, A. (1999), A simple predictive model for the structure of the oceanic pycnocline. *Science*, **283**, 2077–2079.

Griffies, S.M., A. Gnanadesikan, R. C. Pacanowski, V. D. Larichev, J. K. Dukowicz, R. D. Smith (1998), Isoneutral Diffusion in a z-Coordinate Ocean Model. *Journal of Physical Oceanography*, **28:5**, 805–830

Griffies, S.M., R. C. Pacanowski, R. W. Hallberg (2000), Spurious Diapycnal Mixing Associated with Advection in a z-Coordinate Ocean Model. *Monthly Weather Review*, **128:3**, 538–564

Hansen, J., and M. Sato (2004), Greenhouse gas growth rates. *Proc. Natl. Acad. Sci.*, USA 101, 16109–16114.

Ito, T., J. Marshall, and M. Follows (2004), What controls the uptake of transient tracers in the Southern Ocean? *Glob. Biogeochem. Cycles*, **18**, GB2021, doi:10.1029/2003GB002103.

Jayne, S.R. (2009) The Impact of Abyssal Mixing Parameterizations in an Ocean General Circulation Model. *J. Phys. Oceanogr.*, **39**, 1756–1775.

Keller, K., Tan, K., Morel, F.M.M. and Bradford, D.F. (2000), 'Preserving the ocean circulation: Implications for climate policy'. *Climatic Change*, **47**, 17–43.

Keller, K., C. Deutsch, M. G. Hall and D. F. Bradford (2007), Early detection of changes in the North Atlantic meridional overturning circulation: Implications for the design of ocean observation systems. *J. Climate*, **20**, 145–157.

Key, R.M., A. Kozyr, C.L. Sabine, K. Lee, R. Wanninkhof, J. Bullister, R.A. Feely, F. Millero, C. Mordy, T.-H. Peng (2004), A global ocean carbon climatology: Results from Global Data Analysis Project (GLODAP). *Glob. Biogeochem. Cycles*, **18**(4), GB4031, doi: 10.1029/2004GB002247.

Koch, D., D. Jacob, I. Tegen, D. Rind, and M. Chin (1999), Tropospheric sulfur simulation and sulfate direct radiative forcing in the Goddard Institute for Space Studies general circulation model, *J. Geophys. Res.- Atmos.*, 104 (D19), 23,799–23,822.

Large, W. G., J. C. McWilliams, and S. C. Doney (2004), Oceanic vertical mixing: a review and a model with nonlocal boundary layer parameterisation, *Rev. Geophys.*, **32**, 363–403.

Ledwell, J. R., A. J. Watson, and C. S. Law (1993), Evidence for slow mixing across the pycnocline from an open-ocean tracer-release experiment. *Nature*, **364**, 701–703.

Locarnini, R. A., A. V. Mishonov, J. Antonov, T. Boyer, and H. E. Garcia (2006), World Ocean Atlas 2005. Volume **1**: Temperature, 182 pp, U.S. Government Printing Office, Washington, D.C.

Lu, Nelson and Zimmerman, Dale L. (2005), The likelihood ratio test for a separable covariance matrix. *Stat. & Prob. Lett.*, **73**(4), 449–457

Lumpkin, R. and K. Speer (2003), Large-scale vertical and horizontal circulation in the North Atlantic Ocean. *J. of Phys. Oceanogr.*, **33**(9), 1902–1920.

Marotzke J., 1997: Boundary mixing and the dynamics of three-dimensional thermohaline circulation. *J. Phys. Oceanogr.*, **27**, 1713–1728.

Matsumoto, K. and R. M. Key (2004), Natural Radiocarbon Distribution in the Deep Ocean. *Global Environmental Change in the Ocean and on Land*, Eds., M. Shiyomi et al., pp. 45–58.

McManus, J.F., Francois, R., Gherardi, J.M., Keigwin, L.D. and Brown-Leger, S. (2004), Collapse and rapid resumption of Atlantic meridional circulation linked to deglacial climate changes. *Nature*, **428**, 834–837.

Meehl, G.H., T.F. Stocker, W.D. Collins, P. Friedlingstein, A.T. Gaye, J.M. Gregory, A. Kito, R. Knutti, J.M. Murphy, A. Noda, S.C.B. Raper, I.G. Watterson, A.J. Weaver and Z.-C. Zhao (2007), Global climate projections. *Climate Change 2007: The Physical Science Basis.* Contribution of Working Group I to the Fourth Assessment Report of the Intergovernmental Panel on Climate Change, S. Solomon, D. Qin, M. Manning, Z. Chen, M. Marquis, K.B. Averyt, M. Tignor and H.L. Miller, Eds., Cambridge University Press, Cambridge, 747–846.

Metropolis, N., A.W. Rosenbluth, M.N. Rosenbluth, A. H. Teller and E. Teller (1953), Equation of state calculations by fast computing machines. *J. of Chem. Phys.*, **21**, 1087–1092.

Moum, J.N. and W.D. Smyth, 2001: "Upper Ocean Mixing", Encyclopedia of Ocean Sciences, Academic Press. Available at: http://salty.oce.orst.edu/ smyth/papers/UpOcMixing.pdf

Munk W. and Wunsch, C. (1998), Abyssal Recipes-II: Energetics of Tidal and Wind Mixing. *Deep Sea Res.*, **13**, 1977–2010

Naveira Garabato, A. C., K. L. Polzin, B. A. King,, K. J. Heywood and M. Visbeck (2004), Widespread intense turbulent mixing in the Southern Ocean, *Science*, **303**, 210–213.

Pacanowski, R., and S.G.H. Philander (1981), Parameterization of vertical mixing in numerical models of tropical oceans. *J. Phys. Oceanogr.*, **11**, 1443–1451.

Pacanowski, R.C. (1995), MOM 2 documentation: Users guide and reference manual, Version 1.0. GFDL Ocean Group Technical Report No. 3, Geophysical Fluid Dynamics Laboratory, Princeton, New Jersey.

Patwardhan, A., S. Semenov, S. Schneider, I. Burton, C. Magadza, M. Oppenheimer, B. Pittock, A. Rahman, J. Smith, A. Suarez, F. Yamin, K. Keller, A Todorov, A. Finkel, D. MacMynowski, M. Mastrandrea, M. Fuessel, J. Corfee-Morlot, R. Sukumar, J.-P. van Ypersele, and J. Zillman (2007), Assessing key vulnerabilities and the risk from climate change, Chapter 19 in the Intergovernmental Panel on Climate Change Fourth Assessment Report, Working group II: Impacts, Adaptation and Vulnerability, Cambridge University Press.

Saenko, O. A. and A. J. Weaver (2004), What drives heat transport in the Atlantic: Sensitivity to mechanical energy supply and buoyancy forcing in the Southern Ocean. *Geophysical Research Letters*, **31**, L20305, doi:10.1029/2004GL020671.

Sato, M., J.E. Hansen, M.P. McCormick, and J.B. Pollack (1993), Stratospheric aerosol optical depth, 1850–1990. *J. Geophys. Res.*, **98**, 22987–22994.

Schmittner, A., N.M. Urban, K. Keller, and D. Matthews (2009), Using tracer observations to reduce the uncertainty of ocean diapycnal mixing and climate carbon-cycle projections. *Global Bio. Cycles.*, in press, available at http:/www.geosc.psu.edu/∼kkeller.

Schmittner, and A. J. Weaver (2001), Dependence of multiple climate states on ocean mixing parameters. *Geophys. Res. Lett.,* **28**, 1027–1030.

Schmittner, A., A. Oschlies, X. Giraud, M. Eby, and H. L. Simmons (2005), A global model of the marine ecosystem for long-term simulations: Sensitivity to ocean mixing, buoyancy forcing, particle sinking, and dissolved organic matter cycling. *Glob. Biogeochem. Cycles*, **19**(3), GB3004, doi: 10.1029/2004GB002283.

Simmons, H. L., S. Jayne, L. St. Laurent, A. Weaver (2004), Tidally driven mixing in a numerical model of the ocean general circulation, *Ocean Modelling*, **6** (3-4), 245–263,

ISSN 1463-5003, DOI: 10.1016/S1463-5003(03)00011-8.

Smyth, W.D. and J.N. Moum, 2001: "3D Turbulence", Encyclopedia of Ocean Sciences, Academic Press. Available at: http://salty.oce.orst.edu/ smyth/papers/OceanTurbulence.pdf

Sokolov, A., C. Wang, G. Holian, P. Stone, and R. Prinn (1998), Uncertainty in the oceanic heat and carbon uptake and its impact on climate projections. *Geophys. Res. Lett.*, **25**, 3603–3606.

Sorensen, J., J. Ribbe, and G. Shaffer (2001), Antarctic intermediate water mass formation in ocean general circulation models. *J. Phys. Oceanogr.*, **31**, 3295–3311.

Sriver, R. L., Goes, M., Mann, M. E.; Keller, K. (2010), Climate response to tropical cyclone-induced ocean mixing in an Earth system model of intermediate complexity. *J. Geophys. Res.*, doi:10.1029/2010JC006106. (in press)

Stein, Michael Leonard (1999), Interpolation of Spatial Data: Some Theory for Kriging, Springer-Verlag Inc., 247 pp.

St. Laurent, L., H. L. Simmons, S. R. Jayne (2002), Estimating tidally driven mixing in the deep ocean. *Geophys. Res. Lett.,* , **29**, 2106–2110, doi:10.1029/2002GL015633.

Stuiver, M. & Polach, H.A (1977), "Discussion: Reporting of 14 C data", Radiocarbon, **19**, no. 3, pp. 355–363.

Toggweiler, J.R., Dixon, K., and Bryan, K. (1989), Simulations of radio–carbon in a coarse–resolution, world ocean model, II. Distributions of bomb–produced ^{14}C. *J. Geophys. Res.*, 94, 8243–8264.

Tomassini, L., P. Reichert, R. Knutti, T. F. Stocker and M. Borsuk (2007), Robust Bayesian uncertainty analysis of climate system properties using Markov chain Monte

Carlo methods, *Journal of Climate*, **20**, 1239–1254.

Weaver, A.J., M. Eby, E. C. Wiebe, C. M. Bitz, P. B. Duffy, T. L. Ewen, A. F. Fanning, M. M. Holland, A. MacFadyen, H.D. Matthews, K.J. Meissner, O. Saenko, A. Schmittner, H. Wang and M. Yoshimori (2001), The UVic Earth System Climate Model: Model description, climatology, and applications to past, present and future climates. *Atmosphere-Ocean*, **39**(4), 361–428.

Wunsch, C., and R. Ferrari (2004), Vertical Mixing, Energy, and the General Circulation of the Oceans. *Ann. Rev. Fluid Mech.*, **36**, 281–314.

Zickfeld, K., A. Levermann, M. Morgan, T. Kuhlbrodt, S. Rahmstorf, and D. Keith (2007), Expert judgements on the response of the Atlantic meridional overturning circulation to climate change. *Climatic Change*, **82**, 235–265

Zickfeld, K., M. Eby, and A.J. Weaver (2008), Carbon-cycle feedbacks of changes in the Atlantic meridional overturning circulation under future atmospheric CO2. *Glob. Biogeochem. Cycles*, **22**, GB3024, doi:10.1029/2007GB003118.

List of Figure Captions

622 **Figure 1.** AMOC strength (Sv), defined as the maximum of the transport streamfunc-

623 tion, from years 1800 to 2200. Dashed lines are for the ENSEMBLE 1 ($u\_K_{SO} = 0$); solid

624 lines are for the ENSEMBLE 2 ($u\_K_{SO} = 1$).

625 **Figure 2.** Zonal averages for the Atlantic Ocean of CFC-11 concentration in [pmol/Kg]

626 (colorbars) and density anomalies in [Kg/m^3] (contour lines) for the model with diffu-

627 sivity of K_{bg} =0.05 (top panels) and K_{bg} =0.5 (middle panels). The left column is for

628 ENSEMBLE 1 (u_K_{SO}=0) and right column for ENSEMBLE 2 (u_K_{SO}=1). The bottom

629 panel shows the observations from [*Key et al.*, 2004] and [*Locarnini et al.*, 2006].

630 **Figure 3.** Zonal averages for the Atlantic Ocean of Δ^{14}C concentration in permil (col-

631 orbars) and density anomalies in [Kg/m^3] (contour lines) for the model with diffusivity of

632 K_{bg} =0.05 (top panels) and K_{bg} =0.5 (middle panels). The left column is for ENSEMBLE

633 1 (u_K_{SO}=0) and right column for ENSEMBLE 2 (u_K_{SO}=1). The bottom panel shows

634 the observations from [*Key et al.*, 2004] and [*Locarnini et al.*, 2006].

635 **Figure 4.** Global averaged profiles of CFC-11 [*Key et al.*, 2004], Δ^{14}C [*Key et al.*, 2004]

636 and T [*Locarnini et al.*, 2006], for the observations (gray dots) and model ENSEMBLE 1

637 (colored lines). The legend for the model K_{bg} values is the same as in Figure 1.

638 **Figure 5.** Sensitivity of the model parameter estimation to different treatments of

639 structural model errors. Shown are the posterior probability density function of Δ^{14}C

640 (red lines with crosses) and T (blue lines with circles), and the joint posterior using both

observations (black line with squares). The panels are for the cases discussed in the text:

a) $[\mu = b, \rho = 0]$; b) $[\mu = b, \rho = \hat{\rho}]$; c) $[\mu = az + b, \rho = 0]$; d) $[\mu = az + b, \rho = \hat{\rho}]$.

Figure 6. Posterior probability density function of the model parameters for all considered sources of information, the joint posterior using all available information from observations (line with squares). The climatological AMOC estimate of [*Lumpkin & Speer*, 2003] is plotted for comparison (line with triangles). The K_{bg} estimates are for a) ENSEMBLE 1, b) ENSEMBLE 2, c) ENSEMBLE 1 + ENSEMBLE 2; d) the u_K_{SO} estimate is for ENSEMBLE 1 + ENSEMBLE 2

Figure 7. Joint posterior probability density function of model projections of the maximum AMOC strength in the years 2000, 2100 and 2200 using information from the Δ^{14}C, CFC-11 and T observations. The climatological AMOC estimate of [*Lumpkin & Speer*, 2003] is added for comparison (line with triangles).

Table 1. Properties of the statistical distributions of the sensitivity test for the best K_{bg}: mode, bias ($\mu = az + b$), standard deviation and cross-correlation of residuals for Δ^{14}C and T, and mode of the posterior (joint distribution considering all tracers information).

Exp.	Mode (cm^{2}s^{-1})		bias (a,b)		σ		Cross-corr.	Mode of
	Δ^{14}C	T	Δ^{14}C	T	Δ^{14}C	T	at best K_{bg}	posterior
a)	0.3	0.4	(-14.0,0)	(0.45,0)	12.5	0.6	–	0.3
b)	0.3	0.4	(-14.0,0)	(0.45,0)	12.5	0.6	0.70	0.2
c)	0.15	0.2	(-16.1,9e-3)	(0.22,3.3e-4)	7.7	0.28	–	0.15
d)	0.15	0.2	(-16.1,9e-3)	(0.22,3.2e-4)	7.7	0.28	0.40	0.15

Table 2. Properties of the statistical distributions (mode, mean and 95% credible interval [CI] (cm^{2}s^{-1})) of K_{bg} (Figure 6c) for each considered sources of information, the posterior (joint distribution considering all tracers information), and the climatological AMOC estimate (*Lumpkin & Speer* [2003]). Also shown are the cross-tracers correlation at the best K_{bg} value estimated in the joint posterior.

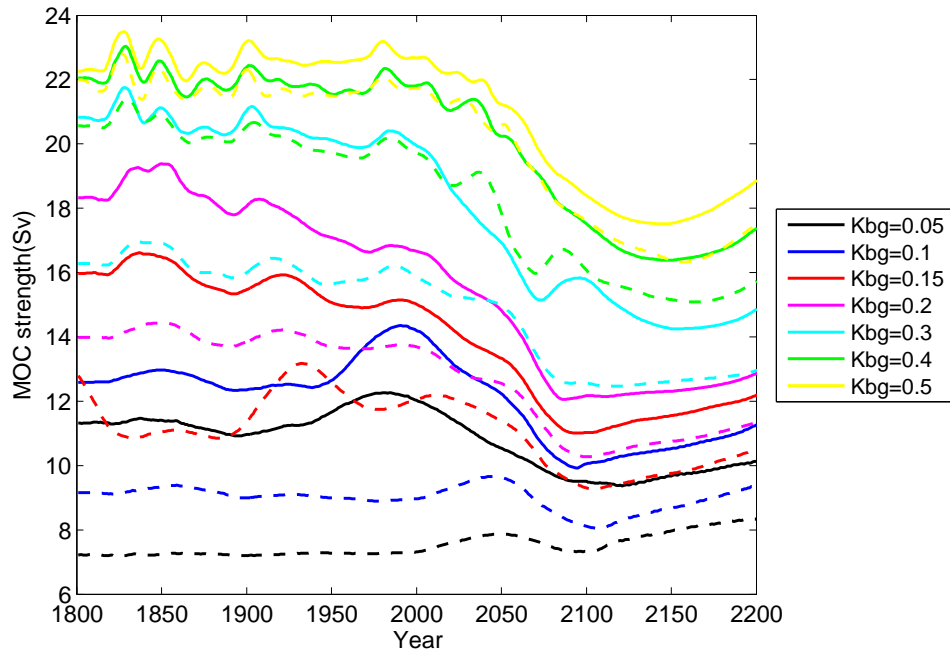| Observation	Mode	Mean	95% CI	Cross-corr. at best K_{bg}		
				Δ^{14}C	CFC-11	T
Δ^{14}C	0.15	0.15	0.22	1	0.06	0.38
CFC-11	0.20	0.23	0.26	–	1	0.02
T	0.15	0.18	0.26	–	–	1
posterior	0.15	0.16	0.17	–	–	-
AMOC clim	0.20	0.20	0.42	–	–	-

Figure 1.   AMOC strength (Sv), defined as the maximum of the transport streamfunction, from years 1800 to 2200. Dashed lines are for the ENSEMBLE 1 ($u\_K_{SO} = 0$); solid lines are for the ENSEMBLE 2 ($u\_K_{SO} = 1$).
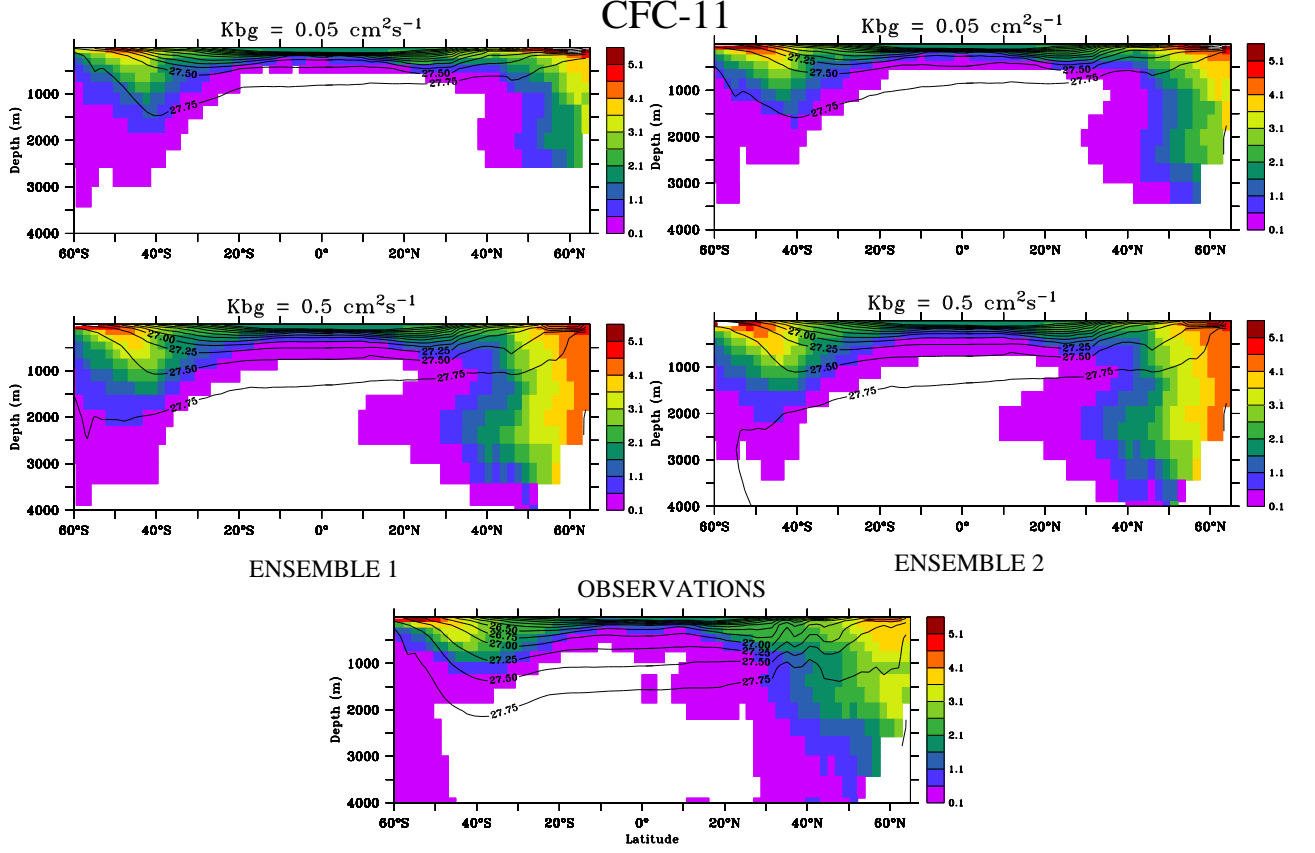
Figure 2. Zonal averages for the Atlantic Ocean of CFC-11 concentration in [pmol/Kg] (colorbars) and density anomalies in [Kg/m³] (contour lines) for the model with diffusivity of K_{bg} =0.05 (top panels) and K_{bg} =0.5 (middle panels). The left column is for ENSEMBLE 1 (u_K_{SO}=0) and right column for ENSEMBLE 2 (u_K_{SO}=1). The bottom panel shows the observations from [*Key et al.*, 2004] and [*Locarnini et al.*, 2006].
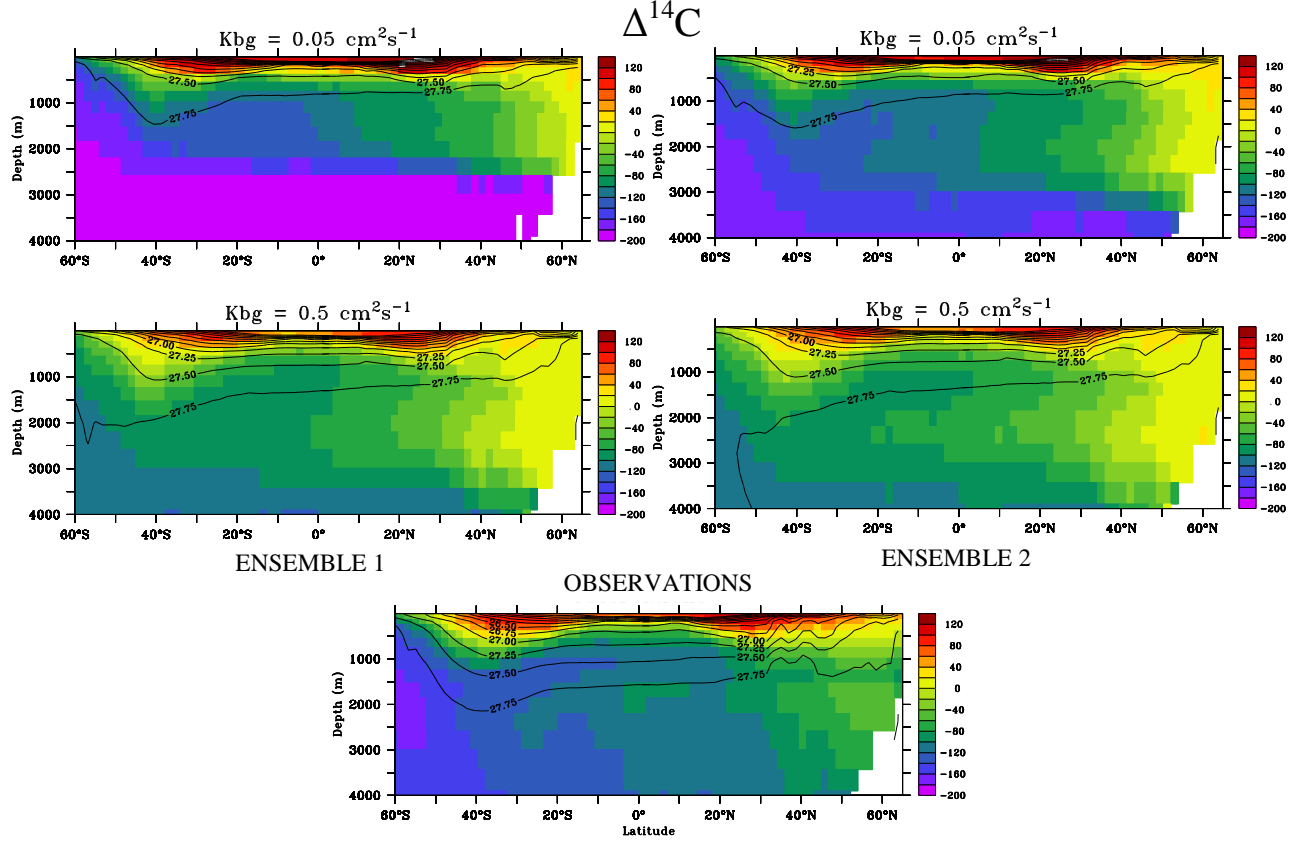
Figure 3. Zonal averages for the Atlantic Ocean of $\Delta^{14}C$ concentration in permil (colorbars) and density anomalies in [Kg/m^3] (contour lines) for the model with diffusivity of K_{bg} =0.05 (top panels) and K_{bg} =0.5 (middle panels). The left column is for ENSEMBLE 1 (u_K_{SO}=0) and right column for ENSEMBLE 2 (u_K_{SO}=1). The bottom panel shows the observations from [*Key et al.*, 2004] and [*Locarnini et al.*, 2006].
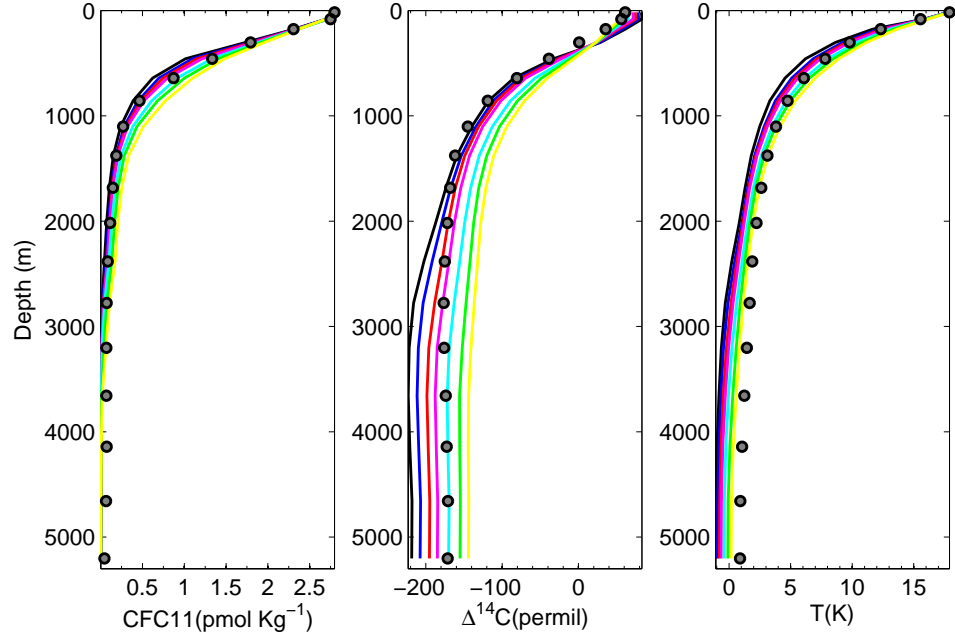
Figure 4. Global averaged profiles of CFC-11 [*Key et al.*, 2004], Δ^{14}C [*Key et al.*, 2004] and

T [*Locarnini et al.*, 2006], for the observations (gray dots) and model ENSEMBLE 1 (colored

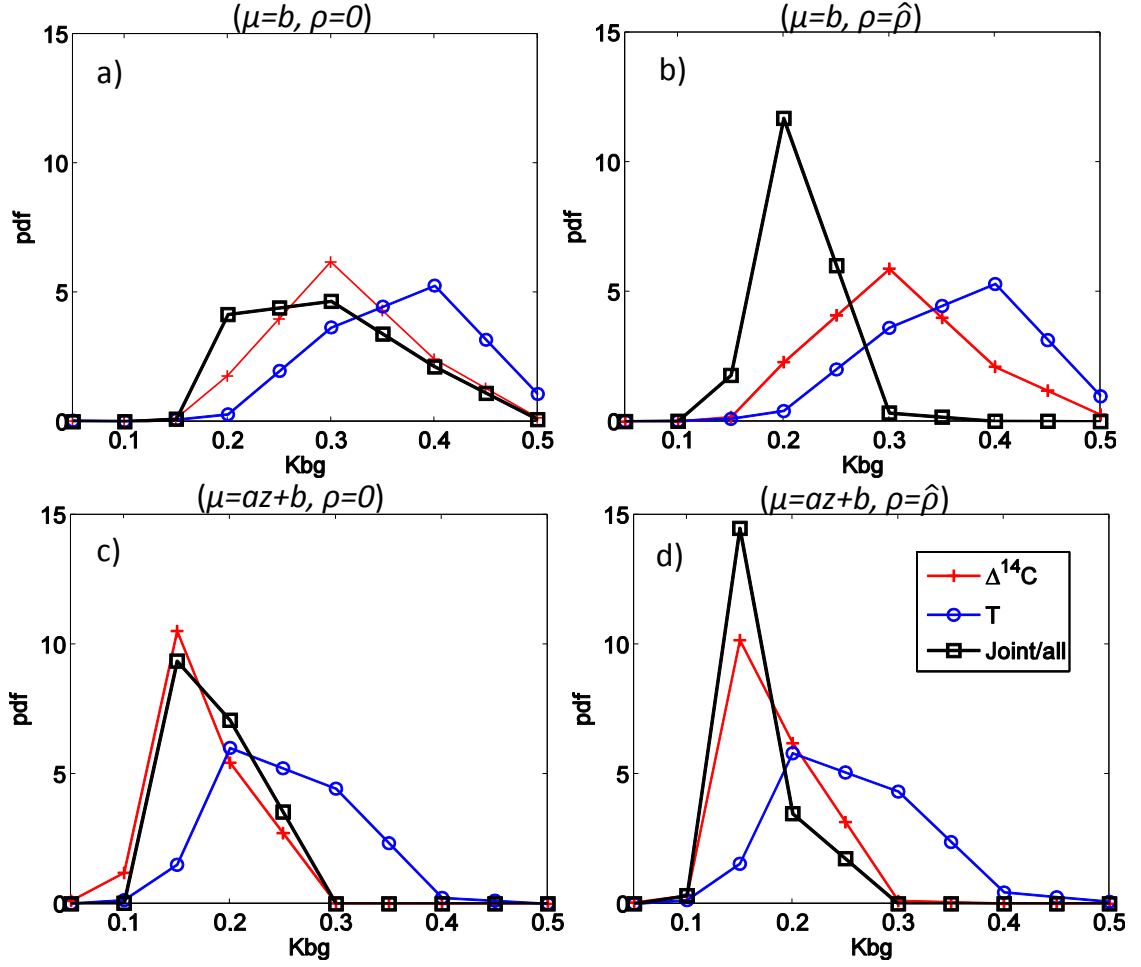lines). The legend for the model K_{bg} values is the same as in Figure 1.

Figure 5. Sensitivity of the model parameter estimation to different treatments of structural model errors. Shown are the posterior probability density function of Δ^{14}C (red lines with crosses) and T (blue lines with circles), and the joint posterior using both observations (black line with squares). The panels are for the cases discussed in the text: a) $[\mu = b, \rho = 0]$; b) $[\mu = b, \rho = \hat{\rho}]$; c) $[\mu = az + b, \rho = 0]$; d) $[\mu = az + b, \rho = \hat{\rho}]$.
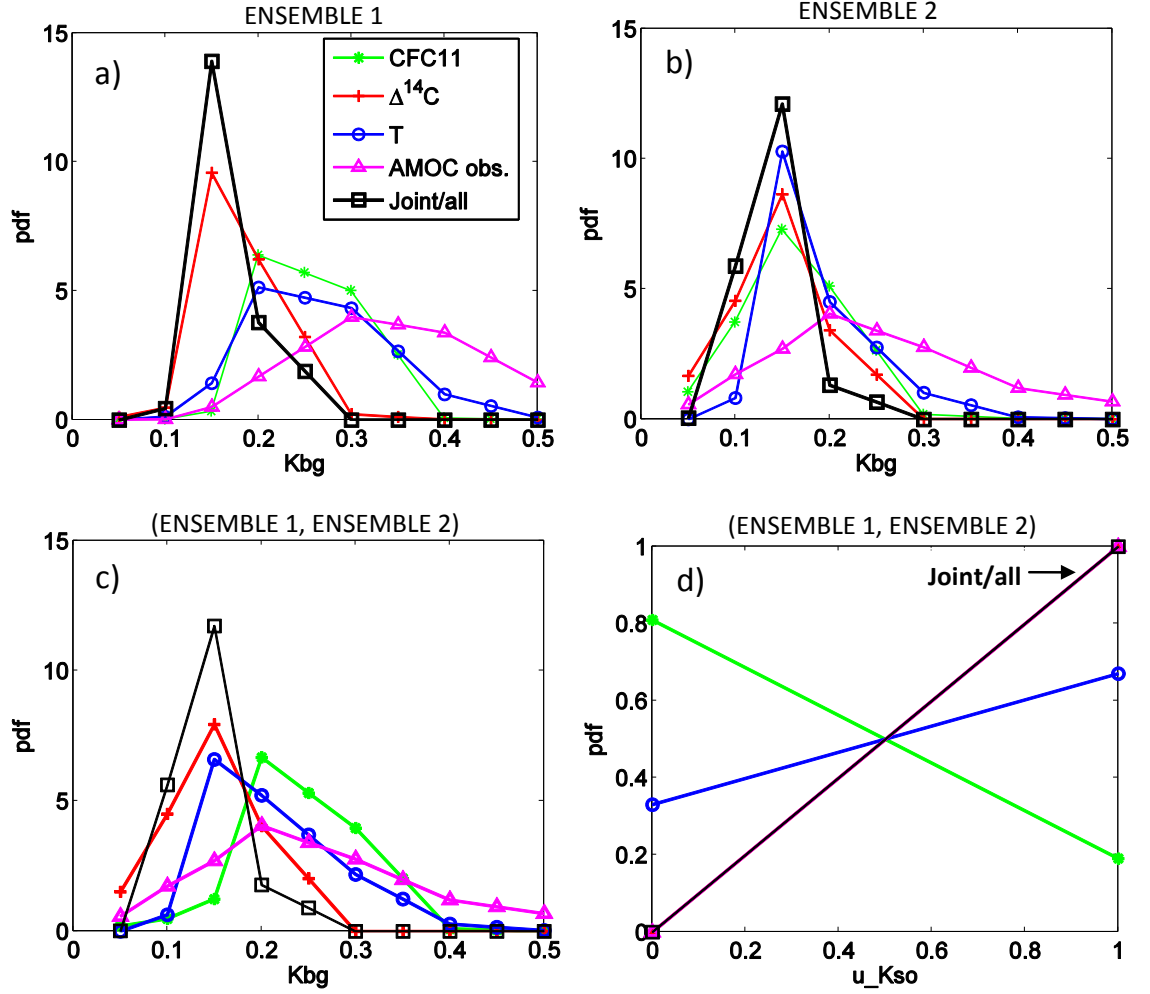
Figure 6. Posterior probability density function of the model parameters for all considered sources of information, the joint posterior using all available information from observations (line with squares). The climatological AMOC estimate of [*Lumpkin & Speer*, 2003] is plotted for comparison (line with triangles). The K_{bg} estimates are for a) ENSEMBLE 1, b) ENSEMBLE 2, c) ENSEMBLE 1 + ENSEMBLE 2; d) the u_K_{SO} estimate is for ENSEMBLE 1 + ENSEMBLE 2
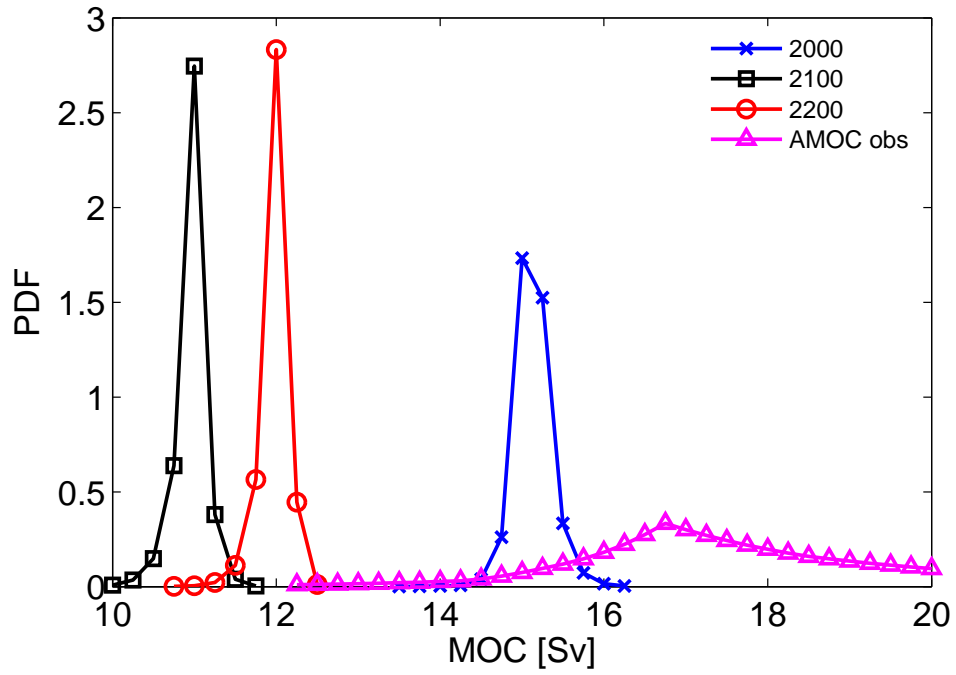
Figure 7. Joint posterior probability density function of model projections of the maximum AMOC strength in the years 2000, 2100 and 2200 using information from the Δ^{14}C, CFC-11 and T observations. The climatological AMOC estimate of [*Lumpkin & Speer*, 2003] is added for comparison (line with triangles).